Microscopic magnetic Hamiltonian for exotic spin textures in metals

Deepak S. Kathyat⬤, Arnob Mukherjee⬤, and Sanjeev Kumar⬤
Department of Physical Sciences, Indian Institute of Science Education and Research (IISER) Mohali,
Sector 81, S.A.S. Nagar, Manauli PO 140306, India

We derive and study a microscopic spin Hamiltonian on a lattice for Rashba-coupled double exchange metals. The Hamiltonian consists of anisotropic interactions of the Dzyaloshinskii-Moriya and pseudodipolar form, in addition to the standard isotropic term. We validate the spin Hamiltonian by comparing results with those on the exact spin-fermion model, and present its phase diagram using large-scale Monte Carlo simulations. In addition to ferromagnetic, planar spiral, and flux states, the model hosts skyrmion crystal and classical spin-liquid states characterized, respectively, by multiple peaks and a diffuse ring pattern in the spin-structure factor. The filamentary domain-wall structures in the spin-liquid state are in remarkable agreement with experimental data on thin films of MnSi-type B20 metals and transition metals and their alloys.

I. INTRODUCTION

The search for magnetic materials supporting unusual spin textures has become an important theme of research in recent years [1–7]. Presence of such textures in insulators and metals holds promise for technological applications [8–10]. In particular, topologically protected magnetic textures such as skyrmions are considered building blocks of racetrack memory devices [11–14]. Presence of such spin textures in metals allows for their control using ultralow currents. Furthermore, noncoplanar magnetic states in metals are known to dramatically influence the spin-polarized charge transport—a feature that can be utilized in spintronics applications [15–21]. There are various metallic magnets, e.g., MnSi, FeGe, Co-Zn-Mn alloys, etc., that support exotic spin textures not only in the ground state but also at higher temperatures [5,22–25]. Similar spin textures are also observed in thin films as well as multilayers involving transition metals [26–31].

The key step toward designing or discovering materials with unconventional spin textures is to understand the physics of minimal microscopic models incorporating essential elementary mechanisms [32–34]. Spin Hamiltonians naturally emerge in insulators as the charge degrees of freedom become inactive and the low-energy physics is determined by the spin degrees of freedom. In contrast, spin Hamiltonians in metals are phenomenologically motivated. Exceptions exist in metals that consist of a subsystem of localized magnetic moments interacting with conduction band. The RKKY model is a famous example in this category [35–39]. Explanation of skyrmionlike spin textures relies on the presence of DM interactions [40–44]. While such anisotropic terms have been motivated by invoking the effect of spin-orbit coupling (SOC) in a two-site setting, a derivation on lattice for the metallic case does not exist [32,45].

In this paper, we present a closed form expression for a spin Hamiltonian for Rashba coupled double-exchange (DE) magnets. The resulting model consists of anisotropic terms resembling Dzyaloshinskii-Moriya (DM) and pseudodipolar interactions on nearest-neighbor (NN) sites with inhomogeneous coupling parameters. After presenting the derivation, we explicitly test the validity of the pure spin model by comparing results against exact diagonalization-based simulations on the starting electronic model. The magnetic phase diagram of the spin model is obtained via large-scale Monte Carlo simulations. The model supports, in addition to a ferromagnetic (FM) phase, (i) single-Q (SQ) spiral states, (ii) diagonally oriented flux (d-flux) state, (iii) multiple-Q (MQ) states with noncoplanar skyrmion crystal (SkX) patterns, and (iv) a classical spin liquid (CSL) state characterized by diffuse ring patterns in the spin structure factor (SSF). The CSL state shows a filamentary domain-wall structure of remarkable similarity to the experimental data on thin films and multilayers of B20 compounds and transition metals [21,27,28]. The spin model introduced here has a wide range of applicability as it originates from the FM Kondo lattice model (FKLM)—a generic model for metals with local moments. Some of the well-known families of materials where FKLM is realized are manganites, doped magnetic semiconductors, and Heusler compounds [46–53]. The key ingredient in the model is the Rashba SOC, which requires breaking of inversion symmetry. Such inversion symmetry breaking is naturally achieved for the emergent conduction layers at interfaces or in thin films of magnetic metals [54].

II. DERIVATION OF THE SPIN HAMILTONIAN

Our starting point is the FKLM in the presence of Rashba SOC on a square lattice, described by the Hamiltonian:

$$H = -t \sum_{\langle ij \rangle, \sigma} (c_{i\sigma}^\dagger c_{j\sigma} + \text{H.c.}) + \lambda \sum_i [(c_{i\downarrow}^\dagger c_{i+x\uparrow} - c_{i\uparrow}^\dagger c_{i+x\downarrow})$$

$$+ i(c_{i\downarrow}^\dagger c_{i+y\uparrow} + c_{i\uparrow}^\dagger c_{i+y\downarrow}) + \text{H.c.}] - J_H \sum_i \mathbf{S}_i \cdot \mathbf{s}_i. \quad (1)$$

Here, $c_{i\sigma}(c_{i\sigma}^\dagger)$ annihilates (creates) an electron at site i with spin σ, $\langle ij \rangle$ implies that i and j are NN sites. λ and

J_H denote the strengths of Rashba coupling and FM Kondo (or Hund's) coupling, respectively. $\mathbf{s}_i$ is the electronic spin operator at site i, and $\mathbf{S}_i$, with $|\mathbf{S}_i| = 1$, denotes the localized spin at that site. We parametrize $t = (1 - \alpha)t_0$ and $\lambda = \alpha t_0$ to connect the weak and strong Rashba limits, $\alpha = 0$ and $\alpha = 1$, respectively. $t_0 = 1$ sets the reference energy scale.

Note that coupling between localized spins $\mathbf{S}_i$ is mediated via the conduction electrons. In the limit of weak Kondo coupling, this leads to a modified RKKY Hamiltonian which is discussed in a recent work [55]. To clarify the physics of the above Hamiltonian in the $J_H \to \infty$ limit, also known as the DE limit, we rewrite the Hamiltonian in a basis where the spin-quantization axes are site dependent and align with the direction of the local magnetic moment [56]. Since antiparallel orientations are strongly suppressed for large J_H, the low-energy physics is determined by effectively spinless fermions with the spin quantization axis parallel to the local moments. Projecting onto the parallel subspace, we obtain the Rashba DE (RDE) Hamiltonian,

$$H_{\mathrm{RDE}} = \sum_{\langle ij \rangle, \gamma} \left[g_{ij}^{\gamma} d_{ip}^{\dagger} d_{jp} + \text{H.c.} \right], \qquad (2)$$

where, $d_{ip}(d_{ip}^{\dagger})$ annihilates (creates) an electron at site i with spin parallel to the localized spin. Site $j = i + \gamma$ is the NN of site i along spatial direction $\gamma = x, y$. The projected hopping $g_{ij}^{\gamma} = t_{ij}^{\gamma} + \lambda_{ij}^{\gamma}$ have contributions from the standard hopping integral t and the Rashba coupling λ, and depend on the orientations of the local moments. The two contributions to g_{ij}^{γ} are given by

$$t_{ij}^{\gamma} = -t \left[\cos\left(\frac{\theta_i}{2}\right) \cos\left(\frac{\theta_j}{2}\right) + \sin\left(\frac{\theta_i}{2}\right) \sin\left(\frac{\theta_j}{2}\right) e^{-i(\phi_i - \phi_j)} \right],$$

$$\lambda_{ij}^{x} = \lambda \left[\sin\left(\frac{\theta_i}{2}\right) \cos\left(\frac{\theta_j}{2}\right) e^{-i\phi_i} - \cos\left(\frac{\theta_i}{2}\right) \sin\left(\frac{\theta_j}{2}\right) e^{i\phi_j} \right],$$

$$\lambda_{ij}^{y} = i\lambda \left[\sin\left(\frac{\theta_i}{2}\right) \cos\left(\frac{\theta_j}{2}\right) e^{-i\phi_i} + \cos\left(\frac{\theta_i}{2}\right) \sin\left(\frac{\theta_j}{2}\right) e^{i\phi_j} \right].$$
$$(3)$$

Writing g_{ij}^{γ} in the polar form, $g_{ij}^{\gamma} = f_{ij}^{\gamma} e^{ih_{ij}^{\gamma}}$, and defining the ground-state expectation values $D_{ij}^{\gamma} = \langle [e^{ih_{ij}^{\gamma}} d_{ip}^{\dagger} d_{jp} + \text{H. c.}] \rangle_{gs}$ as coupling constants, we obtain the low-energy approximate spin Hamiltonian,

$$H_S = - \sum_{\langle ij \rangle, \gamma} D_{ij}^{\gamma} f_{ij}^{\gamma},$$

$$\sqrt{2} f_{ij}^{\gamma} = [t^2(1 + \mathbf{S}_i \cdot \mathbf{S}_j) + 2t\lambda \hat{\gamma}' \cdot (\mathbf{S}_i \times \mathbf{S}_j)$$
$$+ \lambda^2 (1 - \mathbf{S}_i \cdot \mathbf{S}_j + 2(\hat{\gamma}' \cdot \mathbf{S}_i)(\hat{\gamma}' \cdot \mathbf{S}_j))]^{1/2}, \quad (4)$$

with $\hat{\gamma}' = \hat{z} \times \hat{\gamma}$. We note that the functional form f_{ij}^{γ} was motivated in an earlier paper by considering a two-site problem [45]. However, the key argument of performing link-dependent SU(2) rotations to gauge away the Rashba term works only for two isolated sites and cannot be generalized to a lattice. Our derivation is free from such limitations, and provides a model where D_{ij}^{γ} in Eq. (4) need not be uniform [56].
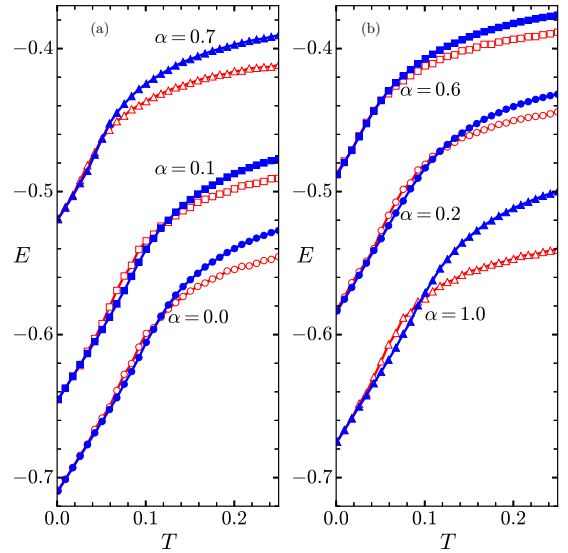

FIG. 1. (a), (b) Temperature dependence of energy per site obtained via EDMC simulations of H_{RDE} (open symbols) and that obtained via classical Monte Carlo on H_S (filled symbols) for the values of α indicated in the panels. Simulations are carried out on 8×8 lattices.

III. COMPARISON WITH THE EXACT ELECTRONIC MODEL

The key question is how well H_S Eq. (4) describes the low-energy magnetic states of the spin-fermion model H_{RDE}. We directly address this by comparing energetics of the two models in the low-temperature regime. Hybrid simulations combining exact diagonalization and Monte Carlo (EDMC) are carried out for H_{RDE} at electronic filling fraction of $n = 0.3$ [46,57]. Results are compared with simulations on H_S using D_{ij}^{γ} as coupling constants. Energy per site E is defined as statistical average $\overline{H_S}/N$ for the pure spin model and as quantum statistical average $\overline{\langle H_{\mathrm{RDE}} \rangle}/N$ for the spin-fermion model, where the bar denotes the averaging over Monte Carlo steps and N is the number of lattice sites. Comparison of energy per site with varying temperature is shown for representative values of α [see Figs. 1(a)–1(b)]. Ground states are correctly captured by H_S for all choices of α, and the energies between H_{RDE} and H_S match very well in the low-temperature regime. The quantitative agreement can be further improved by using simulation techniques already known for DE systems [58,59]. Incidentally, most of the ground states obtained in EDMC on H_{RDE} lead to narrow distributions of D_{ij}^{γ} [56]. This motivates a simplified approximate spin Hamiltonian with $D_{ij}^{\gamma} \equiv D_0$ in Eq. (4).

IV. MAGNETIC PHASES OF THE NEW SPIN HAMILTONIAN

To investigate the magnetic phase diagram of the spin Hamiltonian Eq. (4) with $D_{ij}^{\gamma} \equiv D_0 = 1$, we use classical Monte Carlo simulations with the standard Metropolis algorithm. The simulations are carried out on lattice sizes varying from $N = 40^2$ to $N = 200^2$, and $\sim 5 \times 10^4$ Monte Carlo steps are used for equilibration and averaging at each temperature
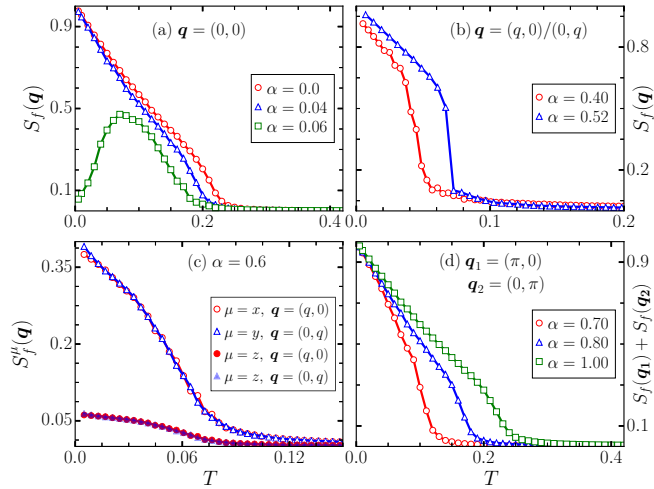
FIG. 2. (a)–(d) Temperature dependence of different components of SSF for representative values of α. Results are obtained on 60×60 lattice.

point. A consistency check on the stability of ground states is performed for simulations on the exact spin Hamiltonian Eq. (4) by recalculating D_{ij}^{γ}. We emphasize that the exact match of ground-state energies between the electronic and the effective spin Hamiltonian, as shown in Fig. 1, is achieved only when inhomogeneities in D_{ij}^{γ} are retained. The different magnetic phases are characterized with the help of a component-resolved SSF,

$$S_f^{\mu}(\mathbf{q}) = \frac{1}{N^2} \sum_{ij} \overline{S_i^{\mu} S_j^{\mu}} \, e^{-i\mathbf{q}\cdot(\mathbf{r}_i - \mathbf{r}_j)}, \qquad (5)$$

where, $\mu = x, y, z$ denotes the component of the spin vector and $\mathbf{r}_i$ is the position vector for spin $\mathbf{S}_i$. The total structure factor can be computed as $S_f(\mathbf{q}) = \sum_{\mu} S_f^{\mu}(\mathbf{q})$. Figure 2 shows the temperature variations of characteristic features in the SSF for different values of α. In the small α regime, the ground state is FM [characterized by $S_f(\mathbf{q})$ at $\mathbf{q} = (0,0)$ in Fig. 2(a)] and the Curie temperature reduces with increasing α. In the large α limit, the d-flux state characterized by simultaneous appearance of peaks at $\mathbf{q} = (\pi, 0)$ and $\mathbf{q} = (0, \pi)$ in SSF is stabilized [see Fig. 3(f)]. The corresponding ordering temperature increases with increasing α [see Fig. 2(d)]. We find two other ordered states at intermediate values of α: SQ spiral states with SSF peaks either at $\mathbf{q} = (q, 0)$ or at $\mathbf{q} = (0, q)$ [see Figs. 2(b) and 3(d)], and noncoplanar MQ states with all three components, $\mu = x, y, z$, contributing to total SSF at different $\mathbf{q}$. For $0.06 \leqslant \alpha \leqslant 0.34$, the SSF displays a circular pattern without any prominent peaks, suggestive of a liquidlike magnetic state [60–62]. The detailed form of SSF for these unusual phases is discussed below.

We summarize the simulation results in the form of a phase diagram in Fig. 3(g). The ground state changes from a FM at small α to a d-flux at large α, via three nontrivial phases for intermediate values of α. The evolution of the ground-state SSF is displayed in Figs. 3(a)–3(f). As the FM state is destabilized upon increasing α, we do not find any ordered phase. Instead, the SSF shows a diffuse circular pattern [see Fig. 3(b)] characteristic of a disordered liquidlike state. The radius of
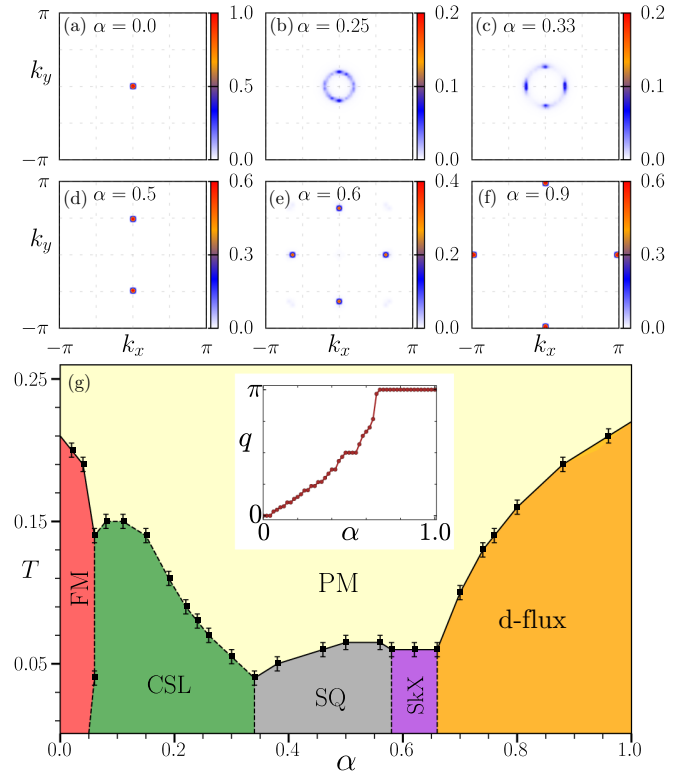

FIG. 3. (a)–(f) Color map of SSF at $T = 0.001$ for different values of α. (g) Phase diagram for the new spin Hamiltonian in the $T - \alpha$ plane. The boundaries are based on the temperature dependence of the relevant components of the SSF. Inset in (g) shows variation in the magnitude q of the relevant wave-vector $\mathbf{q}$ with α.

the ring increases upon increasing α, and the intensity near the axial points, $(\pm q, 0)$ and $(0, \pm q)$, becomes relatively large [see Fig. 3(c)]. For $0.34 < \alpha < 0.58$, we find SQ spiral states with either horizontal or vertical FM stripes [see Figs. 3(d) and 4(c)]. In a narrow window, $0.58 < \alpha < 0.66$, MQ noncoplanar states are stabilized. Finally, the planar d-flux state is obtained as the ground state for $\alpha > 0.66$. Inflection points in the temperature dependence of relevant components of SSF are used to identify the boundaries between the paramagnetic and ordered phases. Note that, in the case of a CSL state, a well-defined order parameter does not exist, and the dashed line indicates the temperature at which the diffuse ring pattern appears in the SSF. The inset in Fig. 3(g) displays the variation of the magnitude q of characteristic wave vector $\mathbf{q}$ with α. We note that the plateau in q near $\alpha = 0.5$, corresponding to $q = \pi/2$ SQ state, and that near $\alpha = 0$, corresponding to the FM phase, disappear in the thermodynamic limit [56].

We provide a clear understanding of the ground-state evolution in terms of typical low-temperature spin configurations in Fig. 4. Upon increasing α, the FM state is destabilized and typical configurations consist of filamentary structures of domain walls [see Figs. 4(a) and 4(b)]. The stability of the filamentary structures is related to an unusual degeneracy of spiral states that originates from the presence of mutually orthogonal directions of the two DM vectors in our spin model [56]. The fact that domain walls can turn in an arbitrary direction with negligible energy costs is responsible for the
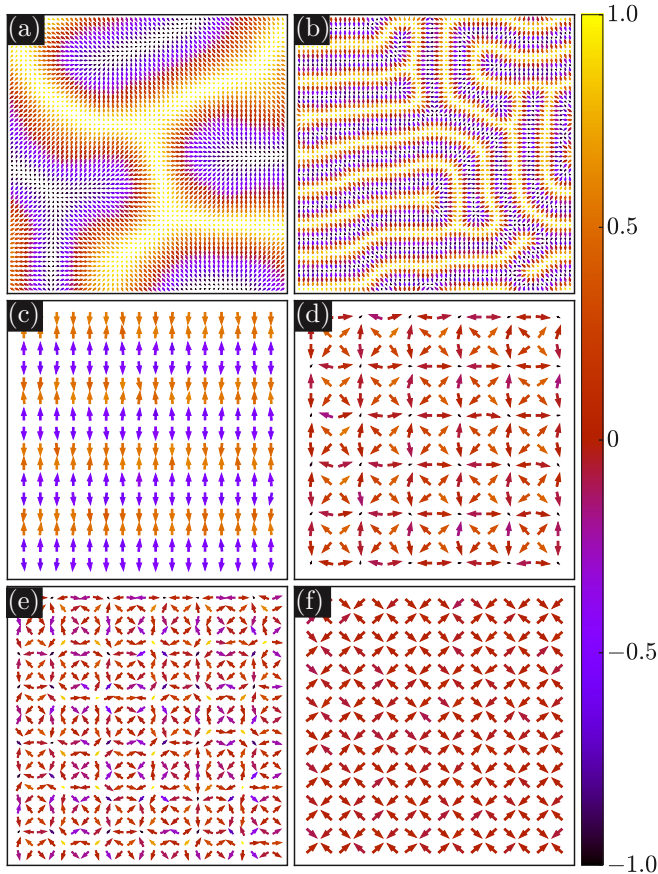
FIG. 4. Snapshots of spin configurations obtained at low temperature for, (a) $\alpha = 0.10$, (b) $\alpha = 0.34$, (c) $\alpha = 0.50$, (d) $\alpha = 0.60$, (e) $\alpha = 0.64$, and (f) $\alpha = 0.80$. The x and y components of the spins are indicated by the arrow while the z component is color coded. For (a) and (b), we show 60×60 lattice. For the ordered states, we display for clarity only a smaller section, 16×16 for (c), (d), and (f) and 24×24 for (e), of the full lattice. The configurations are shown at $T = 0.001$.

presence of the diffuse circular pattern in the SSF [see Fig. 3(b)]. The resulting ground-state degeneracy can be labeled as intermediate between microscopic and macroscopic with the number of degenerate states scaling as $e^{\sqrt{N}}$ as opposed to the well-known e^N in case of macroscopic degeneracy [63]. For larger values of α, the width of domain walls decreases and a preference for horizontal or vertical orientations of the domain walls is found [see Fig. 4(b)]. This is reflected in the appearance of arc features in SSF near the axial points [see Fig. 3(c)]. For $\alpha > 0.58$, we obtain long-range ordered MQ states. The MQ states can be noncoplanar [see Figs. 4(d)–4(e)]

or coplanar [see Fig. 4(f)]. The noncoplanar patterns in the MQ states are identical to lattices of smallest skyrmions [64].

V. CONCLUSION

We have derived a spin Hamiltonian on a lattice for DE metals in the presence of Rashba SOC. The model, in general, has inhomogeneous coupling constants and anisotropic DM and pseudodipolar interactions, similar to those required for stabilizing exotic spin textures. We explicitly compare the energetics in the low-temperature regime between the exact Hamiltonian and our spin model in order to prove the validity of the latter. Increasing the relative strength of Rashba term with respect to the hopping generates CSL, SQ spiral, and MQ SkX states, starting from the trivial FM phase. An elegant description of this evolution emerges from the ground-state degeneracy analysis. Our spin model provides a consistent description of spin textures in itinerant magnets. In particular, the filamentary domain-wall structures obtained in our simulations are in excellent agreement with the experimental observations in thin films and multilayers of transition metals [21,27,28,30,31,65]. Typically, one would associate such irregular spin textures to impurities or defects in the samples. However, our microscopic analysis without including any *ad hoc* term in the Hamiltonian shows that these are intrinsic features of the electronic system. While quenched disorder in a real sample may lead to the pinning of these filamentary domains, we predict that in a disorder-free sample a reorientation dynamics of the domain walls should be observed. Interestingly, similar domain patterns were noticed many years back in FM garnet films [66].

The weak coupling approach to understand magnetism in spin-orbit-coupled itinerant magnets is via RKKY-type effective models [55]. Such models are long ranged and strongly depend on the filling fraction of the conduction band. In contrast, the form of the spin Hamiltonian discussed here is independent of the electronic filling fraction. Therefore, in our description, the exotic magnetic states do not originate from Fermi surface nesting features. Consequently, such states are expected without fine-tuning of electron density. This is consistent with the fact that such spin textures are experimentally observed in a variety of thin films and multilayers of transition metals. While the model is derived starting from the FKLM, at the mean-field level similar physics should hold for the Hubbard model where localized and itinerant electrons are associated with the same band [67,68].

[1] S. Woo, K. Litzius, B. Krüger, M.-Y. Im, L. Caretta, K. Richter, M. Mann, A. Krone, R. M. Reeve, M. Weigand, P. Agrawal, I. Lemesh, M.-A. Mawass, P. Fischer, M. Kläui, and G. S. Beach, Nat. Mater. **15**, 501 (2016), arXiv:1502.07376.

[2] X. Z. Yu, W. Koshibae, Y. Tokunaga, K. Shibata, Y. Taguchi, N. Nagaosa, and Y. Tokura, Nature **564**, 95 (2018).

[3] X. Z. Yu, Y. Onose, N. Kanazawa, J. H. Park, J. H. Han, Y. Matsui, N. Nagaosa, and Y. Tokura, Nature **465**, 901 (2010).

[4] M. Hoffmann, B. Zimmermann, G. P. Müller, D. Schürhoff, N. S. Kiselev, C. Melcher, and S. Blügel, Nat. Commun. **8**, 308 (2017).

[5] A. K. Nayak, V. Kumar, T. Ma, P. Werner, E. Pippel, R. Sahoo, F. Damay, U. K. Rößler, C. Felser, and S. S. P. Parkin, Nature **548**, 561 (2017).

[6] T. Kurumaji, T. Nakajima, V. Ukleev, A. Feoktystov, T. H. Arima, K. Kakurai, and Y. Tokura, Phys. Rev. Lett. **119**, 237201 (2017), arXiv:1710.04000.

[7] N. Kanazawa, J.-H. Kim, D. S. Inosov, J. S. White, N. Egetenmeyer, J. L. Gavilano, S. Ishiwata, Y. Onose, T. Arima, B. Keimer, and Y. Tokura, Phys. Rev. B **86**, 134425 (2012).

[8] A. Fert, N. Reyren, and V. Cros, Nat. Rev. Mater. **2**, 17031 (2017).

[9] N. J. Laurita, G. G. Marcus, B. A. Trump, J. Kindervater, M. B. Stone, T. M. McQueen, C. L. Broholm, and N. P. Armitage, Phys. Rev. B **95**, 235155 (2017).

[10] R. Wiesendanger, Nat. Rev. Mater. **1**, 16044 (2016).

[11] A. Fert, V. Cros, and J. Sampaio, Nat. Nanotechnol. **8**, 152 (2013).

[12] N. Nagaosa and Y. Tokura, Nat. Nanotechnol. **8**, 899 (2013).

[13] B. Göbel, A. Mook, J. Henk, and I. Mertig, Phys. Rev. B **99**, 020405(R) (2019).

[14] K. Karube, K. Shibata, J. S. White, T. Koretsune, X. Z. Yu, Y. Tokunaga, H. M. Rønnow, R. Arita, T. Arima, Y. Tokura, and Y. Taguchi, Phys. Rev. B **98**, 155120 (2018).

[15] T. Zhou, N. Mohanta, J. E. Han, A. Matos-Abiague, and I. Žutić, Phys. Rev. B **99**, 134505 (2019).

[16] J. Kindervater, I. Stasinopoulos, A. Bauer, F. X. Haslbeck, F. Rucker, A. Chacon, S. Mühlbauer, C. Franz, M. Garst, D. Grundler, and C. Pfleiderer, Phys. Rev. X **9**, 041059 (2019).

[17] J. Zang, M. Mostovoy, J. H. Han, and N. Nagaosa, Phys. Rev. Lett. **107**, 136804 (2011).

[18] S. Sorn, S. Divic, and A. Paramekanti, Phys. Rev. B **100**, 174411 (2019).

[19] T. Gao, A. Qaiumzadeh, H. An, A. Musha, Y. Kageyama, J. Shi, and K. Ando, Phys. Rev. Lett. **121**, 017202 (2018).

[20] A. Barcza, Z. Gercsi, K. S. Knight, and K. G. Sandeman, Phys. Rev. Lett. **104**, 247202 (2010).

[21] S. Woo, K. M. Song, X. Zhang, Y. Zhou, M. Ezawa, X. Liu, S. Finizio, J. Raabe, N. J. Lee, S.-I. Kim, S.-Y. Park, Y. Kim, J.-Y. Kim, D. Lee, O. Lee, J. W. Choi, B.-C. Min, H. C. Koo, and J. Chang, Nat. Commun. **9**, 959 (2018).

[22] S. M. Stishov, A. E. Petrova, S. Khasanov, G. K. Panova, A. A. Shikov, J. C. Lashley, D. Wu, and T. A. Lograsso, Phys. Rev. B **76**, 052405 (2007).

[23] X. Z. Yu, N. Kanazawa, Y. Onose, K. Kimoto, W. Z. Zhang, S. Ishiwata, Y. Matsui, and Y. Tokura, Nat. Mater. **10**, 106 (2011).

[24] X. Zhao, C. Jin, C. Wang, H. Du, J. Zang, M. Tian, R. Che, and Y. Zhang, Proc. Natl. Acad. Sci. USA **113**, 4918 (2016).

[25] C. Pfleiderer, D. Reznik, L. Pintschovius, H. v. Löhneysen, M. Garst, and A. Rosch, Nature **427**, 227 (2004).

[26] B. Dupé, M. Hoffmann, C. Paillard, and S. Heinze, Nat. Commun. **5**, 4030 (2014).

[27] S. D. Pollard, J. A. Garlow, J. Yu, Z. Wang, Y. Zhu, and H. Yang, Nat. Commun. **8**, 14761 (2017).

[28] A. Soumyanarayanan, M. Raju, A. L. Gonzalez Oyarce, A. K. C. Tan, M.-Y. Im, A. Petrović, P. Ho, K. H. Khoo, M. Tran, C. K. Gan, F. Ernult, and C. Panagopoulos, Nat. Mater. **16**, 898 (2017).

[29] S. Meyer, M. Perini, S. von Malottki, A. Kubetzka, R. Wiesendanger, K. von Bergmann, and S. Heinze, Nat. Commun. **10**, 3823 (2019).

[30] T. Nagase, M. Komatsu, Y. G. So, T. Ishida, H. Yoshida, Y. Kawaguchi, Y. Tanaka, K. Saitoh, N. Ikarashi, M. Kuwahara, and M. Nagao, Phys. Rev. Lett. **123**, 137203 (2019).

[31] K. Karube, J. S. White, D. Morikawa, C. D. Dewhurst, R. Cubitt, A. Kikkawa, X. Yu, Y. Tokunaga, T.-h. Arima, H. M. Rønnow, Y. Tokura, and Y. Taguchi, Sci. Adv. **4**, eaar7043 (2018).

[32] A. Farrell and T. Pereg-Barnea, Phys. Rev. B **89**, 035112 (2014).

[33] J. P. Chen, D.-W. Zhang, and J. M. Liu, Sci. Rep. **6**, 29126 (2016).

[34] U. K. Rößler, A. A. Leonov, and A. N. Bogdanov, J. Phys. Conf. Ser. **200**, 022029 (2010).

[35] M. A. Ruderman and C. Kittel, Phys. Rev. **96**, 99 (1954).

[36] T. Kasuya, Prog. Theor. Phys. **16**, 45 (1956).

[37] K. Yosida, Phys. Rev. **106**, 893 (1957).

[38] S. Hayami and Y. Motome, Phys. Rev. Lett. **121**, 137202 (2018).

[39] A. V. Bezvershenko, A. K. Kolezhuk, and B. A. Ivanov, Phys. Rev. B **97**, 054408 (2018).

[40] S. Seki, J.-H. Kim, D. S. Inosov, R. Georgii, B. Keimer, S. Ishiwata, and Y. Tokura, Phys. Rev. B **85**, 220406(R) (2012).

[41] S. Seki, X. Z. Yu, S. Ishiwata, and Y. Tokura, Science **336**, 198 (2012).

[42] I. Dzyaloshinsky, J. Phys. Chem. Solids **4**, 241 (1958).

[43] T. Moriya, Phys. Rev. **120**, 91 (1960).

[44] U. K. Rößler, A. N. Bogdanov, and C. Pfleiderer, Nature **442**, 797 (2006).

[45] S. Banerjee, J. Rowland, O. Erten, and M. Randeria, Phys. Rev. X **4**, 031045 (2014).

[46] E. Dagotto, *Nanoscale Phase Separation and Collosal Magnetoresistance* (Springer, Berlin, 2002).

[47] G. Alvarez, M. Mayr, and E. Dagotto, Phys. Rev. Lett. **89**, 277202 (2002).

[48] M. Berciu and R. N. Bhatt, Phys. Rev. Lett. **87**, 107203 (2001).

[49] K. Pradhan and S. K. Das, Sci. Rep. **7**, 9603 (2017).

[50] A. Yaouanc, P. Dalmas de Réotier, B. Roessli, A. Maisuradze, A. Amato, D. Andreica, and G. Lapertot, Phys. Rev. Res. **2**, 013029 (2020).

[51] D. Bombor, C. G. F. Blum, O. Volkonskiy, S. Rodan, S. Wurmehl, C. Hess, and B. Büchner, Phys. Rev. Lett. **110**, 066601 (2013).

[52] C. Felser, L. Wollmann, S. Chadov, G. H. Fecher, and S. S. P. Parkin, APL Mater. **3**, 041518 (2015).

[53] E. Şaşioğlu, L. M. Sandratskii, and P. Bruno, Phys. Rev. B **77**, 064417 (2008).

[54] A. Manchon, H. C. Koo, J. Nitta, S. M. Frolov, and R. A. Duine, Nat. Mater. **14**, 871 (2015).

[55] K. N. Okada, Y. Kato, and Y. Motome, Phys. Rev. B **98**, 224406 (2018).

[56] See Supplemental Material at http://link.aps.org/supplemental/10.1103/PhysRevB.102.075106 for (brief description).

[57] S. Yunoki, J. Hu, A. L. Malvezzi, A. Moreo, N. Furukawa, and E. Dagotto, Phys. Rev. Lett. **80**, 845 (1998).

[58] S. Kumar and P. Majumdar, Eur. Phys. J. B **46**, 315 (2005).

[59] M. J. Calderón and L. Brey, Phys. Rev. B **58**, 3286 (1998).

[60] Y. Tokiwa, J. J. Ishikawa, S. Nakatsuji, and P. Gegenwart, Nat. Mater. **13**, 356 (2014).

[61] H. Okabe, M. Hiraishi, A. Koda, K. M. Kojima, S. Takeshita, I. Yamauchi, Y. Matsushita, Y. Kuramoto, and R. Kadono, Phys. Rev. B **99**, 041113(R) (2019).

[62] S. Nakatsuji, Y. Machida, Y. Maeno, T. Tayama, T. Sakakibara, J. van Duijn, L. Balicas, J. N. Millican, R. T. Macaluso, and J. Y. Chan, Phys. Rev. Lett. **96**, 087204 (2006).

[63] J. W. F. Venderbos, M. Daghofer, J. van den Brink, and S. Kumar, Phys. Rev. Lett. **107**, 076405 (2011).

[64] B. F. McKeever, D. R. Rodrigues, D. Pinna, A. Abanov, J. Sinova, and K. Everschor-Sitte, Phys. Rev. B **99**, 054430 (2019).

[65] S. Woo, K. M. Song, H.-S. Han, M.-S. Jung, M.-Y. Im, K.-S. Lee, K. S. Song, P. Fischer, J.-I. Hong, J. W. Choi, B.-C. Min, H. C. Koo, and J. Chang, Nat. Commun. **8**, 15573 (2017).

[66] M. Seul and D. Andelman, Science **267**, 476 (1995).

[67] I. Martin and C. D. Batista, Phys. Rev. Lett. **101**, 156402 (2008).

[68] K. Pasrija and S. Kumar, Phys. Rev. B **93**, 195110 (2016).